

Seismic velocity and attenuation structures in the top of the Earth's inner core

Lianxing Wen

Department of Geosciences, State University of New York at Stony Brook, Stony Brook, New York, USA

Fenglin Niu

Department of Terrestrial Magnetism, Carnegie Institution of Washington, Washington, D. C., USA

Received 23 January 2001; revised 13 March 2002; accepted 1 May 2002; published 5 November 2002.

[1] We collect a global data set of *PKIKP* and *PKiKP* phases recorded by the Global Seismic Network and many regional seismic arrays to study seismic structure in the top of the Earth's inner core. The *PKIKP* and *PKiKP* observations show different characteristics between those sampling the "eastern" hemisphere (40°E–180°E) of the inner core and those sampling the "western" hemisphere (180°W–40°E). *PKIKP* phases (1) arrive about 0.4 s earlier than the theoretical arrivals based on Preliminary Reference Earth Model (PREM) for those sampling the eastern hemisphere of the inner core and about 0.3 s later for those sampling the western hemisphere (131°–141°); (2) bifurcate at smaller epicentral distances for those sampling the eastern hemisphere, compared to those sampling the western hemisphere; and (3) have smaller amplitudes for those sampling the eastern hemisphere. Waveform modeling of these observations suggests two different types of models for the two "hemispheres" of the top of the inner core, with a model in the eastern hemisphere having a *P* velocity increase of 0.765 km/s across the inner core boundary, a small radial velocity gradient of 0.000055 (km/s)/km, and an average *Q* value of 250, and a model in the western hemisphere with a *P* velocity increase of 0.633 km/s across the inner core boundary, a radial velocity gradient of 0.000533 (km/s)/km and an average *Q* value of 600. The hemispherical difference of seismic structures may be explained by different geometric inclusions of melt and/or different alignments of iron crystals with anisotropic properties in both velocity and attenuation. We speculate that this large-scale pattern of seismic heterogeneities may be caused by a large-scale heat flow anomaly at the bottom of the outer core and/or different vigorousness of convection in the top of the inner core between the two hemispheres. *INDEX TERMS*: 7207 Seismology: Core and mantle; 8124 Tectonophysics: Earth's interior—composition and state; 7203 Seismology: Body wave propagation; 7260 Seismology: Theory and modeling; 5144 Physical Properties of Rocks: Wave attenuation; *KEYWORDS*: inner core, hemisphericity, anisotropy, partial melt, convection, attenuation

Citation: Wen, L., and F. Niu, Seismic velocity and attenuation structures in the top of the Earth's inner core, *J. Geophys. Res.*, 107(B11), 2273, doi:10.1029/2001JB000170, 2002.

1. Introduction

[2] Since *Poupinet et al.* [1983] first observed travel time anomalies associated with *PKIKP* (*PKP_{df}*), a *P* wave transmitting through the inner core, there have been extensive seismic studies on the three-dimensional seismic velocity structures in the inner core. The existence of anisotropy in the inner core is well established by numerous seismic studies from absolute travel time [*Morelli et al.*, 1986; *Shearer*, 1988; *Su and Dziewonski*, 1995], differential travel time [*Creager*, 1992; *Song and Helmberger*, 1995; *McSweeney et al.*, 1997; *Creager*, 1999], and anomalous splitting of core-sensitive modes [*Woodhouse et al.*, 1986; *Tromp*, 1993]. These studies suggest that anisotropy appears to

approximately have an axial symmetry, with *P* velocity being 3% faster in the polar direction than near the equatorial direction. It also now becomes clear that seismic observations demand a much more complicated seismic structure in the inner core. Several studies indicate that anisotropy varies with depth with the top part of the inner core being isotropic or weakly anisotropic [*Shearer*, 1994; *Song and Helmberger*, 1995, 1998]. Many studies also suggest that seismic heterogeneities exist in both global [*Kaneshima*, 1996; *Tanaka and Hamaguchi*, 1997; *Niu and Wen*, 2001] and regional scales [*Cormier and Choy*, 1986; *Creager*, 1997; *Niu and Wen*, 2001]. Seismic attenuation in the inner core is also recognized to be complex by various studies [*Doornbos*, 1974; *Creager*, 1992; *Bhattacharyya et al.*, 1993; *Song and Helmberger*, 1993; *Souriau and Roudil*, 1995; *Souriau and Romanowicz*, 1996; *Cormier et al.*, 1998].

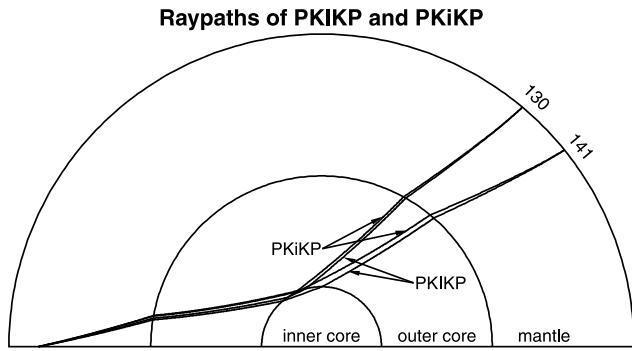


Figure 1. *PKiKP* and *PKIKP* ray paths at the distances of 130° and 141° based on PREM [Dziewonski and Anderson, 1981]. *PKiKP* is the *P* wave reflected off the inner core boundary, and *PKIKP* (*PKP_{df}*) is the *P* wave propagating through the inner core. Note that these two phases have almost identical ray paths in the mantle. The differential travel time and amplitude between the two phases eliminate effects due to uncertainties of source radiation pattern and seismic heterogeneities in the mantle. The waveforms of these phases are most sensitive to the seismic velocity and attenuation structures in the top of the inner core.

[3] At the same time, there is also an extensive search for both microscopic and macroscopic mechanisms for explaining the seismic velocity and attenuation structures, especially the anisotropic velocity structure, of the inner core. The inner core is believed to be composed mostly of iron with hexagonal close-packed (hcp) structure (ϵ -Fe) [Brown and McQueen, 1986; Anderson, 1986]. Both theoretical and experimental studies indicate that the hcp-iron crystals are anisotropic in seismic velocities [Stixrude and Cohen, 1995; Mao et al., 1998, 1999]. The macroscopic mechanisms for producing the observed seismic anisotropy in the inner core

remain unclear. The proposed mechanisms include lattice preferred orientation of the hcp iron crystals by convection in the inner core [Jeanloz and Wenk, 1988; Weber and Machetel, 1992], magnetic field at the inner core boundary [Karato, 1993, 1999], viscous flow induced by preferential growth of the inner core [Yoshida et al., 1996]. Solidification texturing is also suggested as a possible mechanism for generating the anisotropy [Bergman, 1997].

[4] Compared to the deep part of the inner core, there are less systematic studies about the nature of the top of the inner core. Understanding the detailed seismic structure in the top of the inner core, however, could potentially help to distinguish various proposals for the cause of the anisotropy observed in the deep part of the inner core. For example, does the inner core acquire its anisotropy at the time of the solidification or does the inner core anisotropy develop later? If the outermost of the inner core convects, is convection destructive or constructive in developing anisotropy in the inner core? The top of the inner core, by itself, also plays an important role in understanding the thermodynamic process near the inner core boundary, the interaction between the inner and outer core, the growth of the inner core, and the dynamic processes inside the inner core. For example, is the top of the inner core a mushy zone as suggested from the consideration of thermodynamic equilibrium [Fearn et al., 1981], or would the dynamical effects due to compaction exclude the fluid out of the inner core [Sumita et al., 1996]? Is there a large-scale heat flow anomaly, perhaps induced by the core mantle boundary, in the bottom of the outer core? and, does the outermost of the inner core convect?

[5] The lack of knowledge about seismic structure in the top of the inner core will also undoubtedly affect our inference of seismic structures about the deeper portion of the inner core, as any seismic phases sampling the deep part of the inner core will unavoidably propagate through the

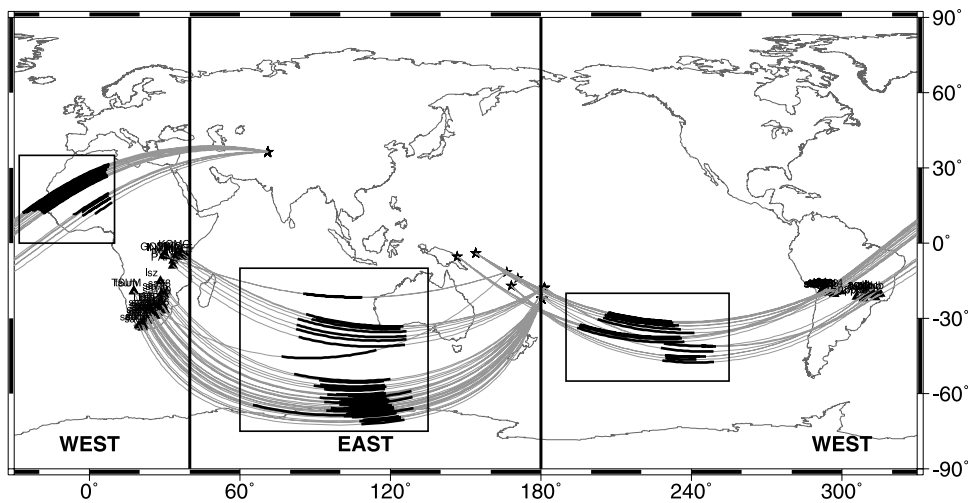


Figure 2. Great circle paths for *PKiKP* and *PKIKP* phases recorded by four regional seismic arrays in southern Africa (the Tanzania Broadband Seismic Experiment and the Kaapvaal Seismic Array) and South America (The Broadband Andean Seismic Experiment and BLSP 94). The heavy lines indicate the *PKIKP* ray paths sampling the inner core. The seismic paths to the South American arrays sample the “western” hemisphere of the inner core, while those to the African arrays sample the “eastern” hemisphere. The geographic separation of the two “hemispheres” is also marked. The record sections of *PKIKP* and *PKiKP* phases are shown in Figures 3a (western) and 3c (eastern).

Table 1. Event List^a

Event	Origin Date	Origin Time	lat	lon	Depth, km
900313	13 March 1990	1940:34.4	-3.42	-76.91	117
900322	22 March 1990	0000:14.4	-36.69	177.27	202
900624	24 June 1990	0835:25.4	-21.50	-176.54	193
900802	2 Aug. 1990	0524:08.9	-31.61	-71.58	41
910409	9 April 1991	0602:25.3	-9.83	-74.78	135
910611	11 June 1991	1432:48.0	-18.13	-178.43	628
911015	15 Oct. 1991	1618:02.6	-6.52	130.07	146
911202	2 Dec. 1991	1727:20.9	-15.89	-69.42	233
911215	15 Dec. 1991	0636:44.7	-30.12	-177.99	104
920102	2 Jan. 1992	1941:45.8	5.66	-73.84	141
920712	12 July 1992	2341:00.0	3.12	122.00	616
920713	13 July 1992	1811:34.0	-3.92	-76.63	100
920815	15 Aug. 1992	1902:09.8	5.08	-75.73	127
920824	24 Aug. 1992	0659:40.5	41.94	140.72	127
920915	15 Sept. 1992	2104:00.9	-14.12	167.26	196
921214	14 Dec. 1992	0741:01.4	-13.97	170.72	634
921223	23 Dec. 1992	0300:45.5	-6.52	130.39	105
921227	27 Dec. 1992	2149:05.4	-6.11	113.06	610
940309	9 March 1994	2328:07.7	-17.77	-178.50	564
940504	4 May 1994	0637:37.9	-17.07	168.27	221
940822	22 Aug. 1994	1726:38.2	-11.50	166.42	148
941025	25 Oct. 1994	0054:34.6	36.30	70.91	244
941218	18 Dec. 1994	2038:32.6	-17.86	-178.69	551
950312	12 March 1995	1209:43.5	-5.33	146.70	233
950624	24 June 1995	0658:06.5	-3.98	153.95	386
950803	3 Aug. 1995	0818:53.5	-28.35	-69.20	104
950817	17 Aug. 1995	2314:19.4	36.47	71.16	239
950824	24 Aug. 1995	0155:34.6	18.92	144.95	589
950824	24 Aug. 1995	0628:54.6	18.88	145.01	600
970101	1 Jan. 1997	2232:32.3	-0.13	123.82	115
970208	8 Feb. 1997	0155:55.7	-8.47	158.96	101
970215	15 Feb. 1997	1211:14.7	-7.78	117.41	274
970311	11 March 1997	0313:59.4	-21.13	-178.86	553
970412	12 April 1997	0921:56.4	-28.17	-178.37	184
970420	20 April 1997	1953:15.5	-34.04	-69.98	105
970517	17 May 1997	0210:18.9	-27.16	-69.50	106
970521	21 May 1997	2251:28.7	23.08	80.04	36
970527	27 May 1997	1509:03.7	16.33	145.44	536
970824	24 Aug. 1997	0059:51.6	13.55	-89.59	139
970826	26 Aug. 1997	1522:09.2	-25.51	178.33	609
970928	28 Sept. 1997	2313:13.9	-22.41	-68.45	106
971008	8 Oct. 1997	1047:49.9	-29.25	178.35	617
971022	22 Oct. 1997	0955:47.8	44.72	146.21	153
971103	3 Nov. 1997	0537:48.7	-20.40	-178.74	600
971106	6 Nov. 1997	1729:07.9	11.69	-85.79	116
971118	18 Nov. 1997	1541:29.6	-29.06	-177.65	52
971128	28 Nov. 1997	0610:47.6	47.14	145.60	393
971129	29 Nov. 1997	0242:27.3	-21.03	-178.76	581
980126	26 Jan. 1998	1830:31.3	-22.04	-176.84	159
980127	27 Jan. 1998	0214:12.9	-20.77	-179.18	642
980207	7 Feb. 1998	0320:18.9	-14.80	167.32	129
980228	28 Feb. 1998	1046:52.3	-14.42	167.35	184
980303	3 March 1998	0224:43.9	14.38	-91.47	62
980325	25 March 1998	2102:55.7	-24.34	-66.99	197
980414	14 April 1998	0341:22.3	-23.82	-179.87	498
980427	27 April 1998	2351:35.7	-6.08	113.10	590
980428	28 April 1998	1544:06.1	-21.97	-179.61	607
980516	16 May 1998	0222:03.2	-22.23	-179.52	586
980516	16 May 1998	1041:28.7	-21.79	-176.64	174
980523	23 May 1998	1744:47.8	8.14	123.73	657
980607	7 June 1998	1610:46.2	-31.52	-67.83	113
980612	12 June 1998	2051:01.8	-24.80	179.83	502
980612	12 June 1998	2153:00.1	-5.72	147.89	139
980828	28 Aug. 1998	1240:58.7	-0.15	125.02	66
980901	1 Sept. 1998	0119:37.5	-17.56	-174.77	219
980902	2 Sept. 1998	1852:42.2	-29.69	-178.79	230
981011	11 Oct. 1998	1204:54.7	-21.04	-179.11	623
981210	10 Dec. 1998	0821:14.5	-7.95	-71.42	649

^aEvents in bold are used in Figures 2, 3a, and 3c.

heterogeneities in the top of the inner core. Indeed, *Niu and Wen* [2001] reports that strong seismic heterogeneities in the top 80 km of the inner core could largely explain the differential *PKPbc-PKPdf* travel time anomalies observed near the equatorial direction [*Tanaka and Hamaguchi*, 1997]. At the same time, the consistency between our observations which sample the top of the inner core [e.g., *Niu and Wen*, 2001] and those sampling the deep part of the inner core [e.g., *Tanaka and Hamaguchi*, 1997] also gives us confidence that these signals indeed originate from the inner core rather than the mantle as argued by *Breger et al.* [2000].

[6] We have done an extensive search for *PKIKP* and *PKiKP* phases recorded in both the Global Seismic Network and many regional seismic arrays. The differential *PKiKP-PKIKP* travel times clearly reveal a difference of seismic velocity between the “western” and “eastern” hemispheres [*Niu and Wen*, 2001]. In this study, we present and discuss in detail the seismic observations sampling these two “hemispheres.” We then explore seismic models from waveform modeling for velocity and attenuation structures appropriate for explaining the seismic data. We also discuss possible interpretations for the inferred seismic structures, as well as possible mechanism for generating the difference of seismic structures between the two hemispheres.

2. Seismic Observations and Detailed Seismic Velocity and Attenuation Structures

[7] The waveform and differential travel time of seismic *PKIKP* and *PKiKP* phases at the distance range between 120° and 141° provide an ideal opportunity to study the seismic structures in the top of the inner core. *PKiKP* is the reflection off the inner core boundary and *PKIKP* is the *P* wave propagating through the inner core (Figure 1). At this distance range (120°–141°), the waveform and differential travel time between these two phases are most sensitive to the seismic velocity and attenuation structures in the top 80 km of the inner core. Their relative amplitude and differential travel time would not be affected by the uncertainties due to source radiation pattern and seismic heterogeneities in the mantle, as both *PKIKP* and *PKiKP* phases have same take-off angles from earthquake source and same incident angles to seismic stations (Figure 1). The effects of seismic structures at the core-mantle boundary are also minor, because the separation between these two phases at the core-mantle boundary is less than 50 km, much less than the Fresnel zones of these two phases. The hit points of *PKIKP* and *PKiKP* phases also overlay each other at the core-mantle boundary for dense array observations [*Niu and Wen*, 2001].

[8] We begin our presentation by showing seismic observations recorded in several regional dense seismic arrays (Figures 2, 3a, and 3c and events in bold in Table 1). The *PKIKP* and *PKiKP* phases recorded in two African seismic arrays and two South American seismic arrays sample the eastern and western hemispheres of the inner core, respectively (Figure 2). All broadband seismograms are filtered with the WWSSN short period instrument response and aligned along the maximum amplitudes of the *PKiKP* phases. Distance corrections are made so that all seismograms are aligned at the distances equivalent to a common

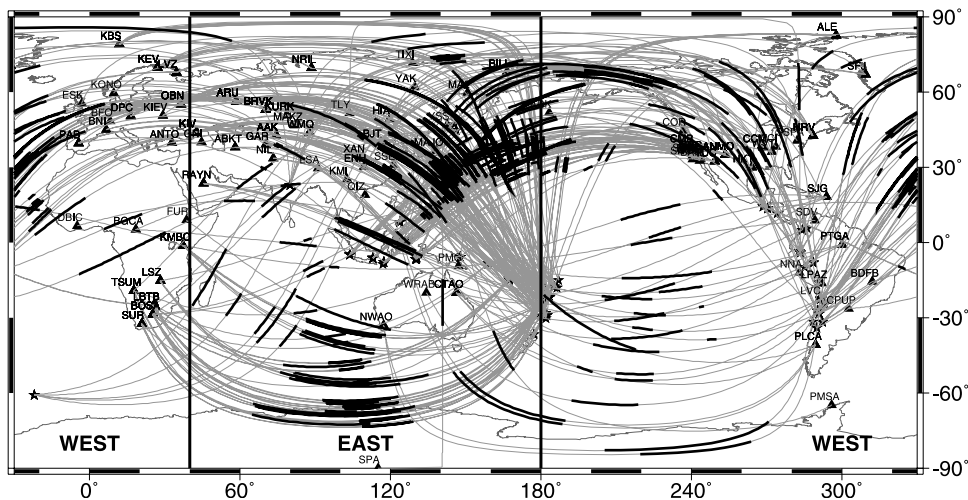


Figure 4. Great circle paths for the *PKIKP* and *PKiKP* phases collected from stations in the global seismic network. The heavy lines represent the *PKIKP* paths in the inner core. The geographic separation of the two hemispheres is also marked. The *PKIKP* and *PKiKP* data sampling these two hemispheres are presented in Figure 6 (eastern) and Figure 5 (western).

source depth of 600 km. When referenced to the *PKiKP* phases, the *PKIKP* phases exhibit different characteristics between those sampling the two hemispheres of the top of the inner core (Figures 3a and 3c). (1) In the distance range of 131° – 141° , *PKIKP* phases sampling the eastern hemisphere of the inner core arrive about 0.4 s earlier than the theoretical arrivals predicted by PREM, whereas those sampling the western hemisphere arrive about 0.3 s later. (2) The bifurcation of the *PKIKP* phase occurs at smaller epicentral distances for those sampling the eastern hemisphere than for those sampling the western hemisphere. (3) *PKIKP*/*PKiKP* amplitude ratios are smaller for the *PKIKP* phases sampling the eastern hemisphere of the inner core.

[9] *PKiKP*-*PKIKP* phases recorded in the Global Seismic Network show same different characteristics for seismic waves sampling the eastern and western hemispheres of the inner core (Figures 4, 5a, 6a, and 6b). Global data are collected from deep moderate earthquakes, covering the period from January 1990 to December 1998 (Figure 4 and Table 1). Every event is checked for the simplicity of source time function. Every seismogram is eye-checked for

its quality. The top of the inner core is reasonably well sampled, although the coverage of the sampling varies from region to region (Figure 4). We hand-pick *PKIKP* and *PKiKP* phases recorded at the distance range of 130° – 141° and report a hemispherical difference of differential *PKiKP*-*PKIKP* travel times in our previous study [Niu and Wen, 2001]. In this study, for the purpose of waveform modeling, we expand our data collection to the distance range of 120° – 141° (Figures 5a, 6a, and 6b). Like those observed in the dense seismic arrays (Figures 3a and 3c), the waveform and the differential travel time of this global collection of *PKiKP*-*PKIKP* data show same characteristics for seismic waves sampling the western and eastern hemispheres of the inner core (Figures 5a, 6a, and 6b). The *PKIKP*/*PKiKP* amplitude ratios observed in this global data set are also systematically larger for seismic waves sampling the western hemisphere of the inner core (Figure 7), similar to those observed in the dense seismic arrays (Figures 3a and 3c).

[10] The above observed waveform and travel time characteristics can be used to place constraints on the

Figure 3. (opposite) (a,c) *PKIKP* and *PKiKP* phases observed in four regional seismic networks (see Figure 2 for great circle paths and geographic locations of the inner core sampled); (b,d) synthetics calculated by the generalized ray theory [Helmberger, 1983] for seismic models appropriate for the two hemispheres of the top of the inner core. All broadband seismograms are filtered with the WWSSN short-period instrument response and aligned along the maximum amplitudes of the *PKiKP* phases. The maximum *PKiKP* amplitudes are impossible to pick at distances less than about 130° for the seismic data sampling the western hemisphere (Figure 3a) and at distances less than about 127° for those sampling the eastern hemisphere (Figure 3c). For those observations, they are aligned by waveform fitting the synthetics based on models E1 (E2) and W1 (W2), respectively. Distance corrections are made so that all seismograms are aligned at the distances equivalent to a common source depth of 600 km. Synthetics for the observations sampling the western hemisphere are calculated using seismic models W1 (heavy traces, Figure 3b) and W2 (dashed traces, Figure 3b) and those for observations sampling the eastern hemisphere are calculated using seismic models E1 (heavy traces, Figure 3d) and E2 (dashed traces, Figure 3d) (see models in Figure 8). The dashed lines are predicted arrivals based on PREM, and the heavy lines mark approximately the arrivals observed in *PKIKP* and *PKiKP* phases. Note that the *PKIKP* phases sampling the eastern hemisphere of the inner core bifurcate in smaller distances, arrive earlier and have smaller amplitudes, than those sampling the western hemisphere. Note also the indistinguishable synthetics produced by models W1, W2 (Figure 3b) and E1, E2 (Figure 3d). A source depth of 600 km is used in the calculations.

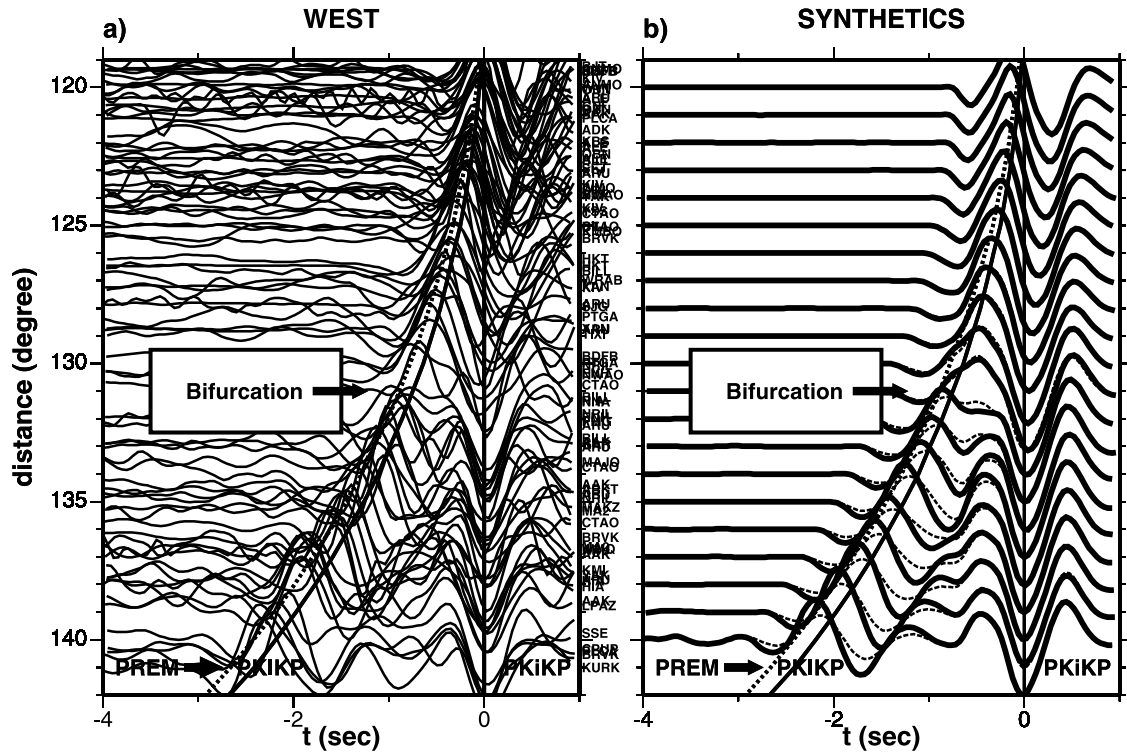


Figure 5. (a) Observed *PKIKP* and *PKiKP* phases sampling the western hemisphere; (b) synthetics calculated from two models with different Q values. The seismic data is collected from the global seismic network (see Figure 4 for great circle paths and the western hemisphere of the inner core sampled). All seismograms are processed and aligned as those in Figure 3a. Distance corrections are made so that all seismic data (Figure 5a) are aligned at the distances equivalent to a common source depth of 600 km. The dash lines are theoretical predicted arrivals based on PREM and the heavy lines mark approximately the arrivals observed in the *PKIKP* and *PKiKP* phases. Note that the data collected in the global seismic network show same characteristics as those recorded in the regional seismic networks (Figure 3a). Synthetics are calculated based on model W1 (heavy traces) and a model with W1 velocity structures and a Q value of 250 (dashed traces). A source depth of 600 km is used in the synthetic calculations.

detailed seismic velocity and attenuation structures in the top of the inner core. Because the hemispherical difference of waveform and travel time is consistently observed in both the global and regional seismic networks, this difference is not caused by lateral variations of seismic structure within the two hemispheres. It is instead indicative of a hemispherical difference of radial velocity and attenuation structures in the top of the inner core. We thus focus our efforts on one dimensional waveform modeling. The bifurcation distance of the *PKiKP* phase and the seismic waveform at the bifurcation distance place tight constraints on the P velocity increase across the inner core boundary. The subsequent move outs and waveshapes of the *PKIKP* phases constrain the radial velocity gradient and Q structure in the top of the inner core. We search velocity and Q models within all ranges of these parameters: the P velocity increase across the inner core boundary, an average Q value in the top of the inner core, the radial velocity gradient in the top of the inner core, and the radial velocity gradient in the bottom of the outer core. We also test the possibility of seismic scattering as an alternative to intrinsic attenuation.

[11] We first fix the seismic velocity structures above the inner core boundary to be PREM values and test different seismic structures in the top of the inner core.

The observations sampling the western hemisphere of the inner core (Figures 3a and 5a) can be explained by a model with a P velocity increase of 0.633 km/s across the inner core boundary, a radial velocity gradient of 0.000533 (km/s)/km and an average Q value of 600 (W1, Figures 8a and 8b), whereas the observations sampling the eastern hemisphere of the inner core (Figures 3c, 6a, and 6b) suggest a P velocity increase of 0.765 km/s across the inner core boundary, a small radial velocity gradient of 0.000055 (km/s)/km, and an average Q structure of 250 (E1, Figures 8a and 8b). Overall, synthetics calculated using models W1 (heavy traces, Figure 3b) and E1 (heavy traces, Figure 3d) match well the observations sampling the western (Figures 3a and 5a) and the eastern (Figures 3c, 6c, and 6d) hemispheres of the inner core.

[12] The inferred seismic velocities in the top of the inner core, however, depend strongly on the assumed seismic structures in the outer core, especially those in the bottom of the outer core. The predicted bifurcation distance and differential *PKiKP*-*PKIKP* travel time are sensitive to the seismic structures in both the top of the inner core and the bottom of the outer core. However, the relative difference of the inferred seismic velocities in the top of the inner core between the two hemispheres is affected little by the

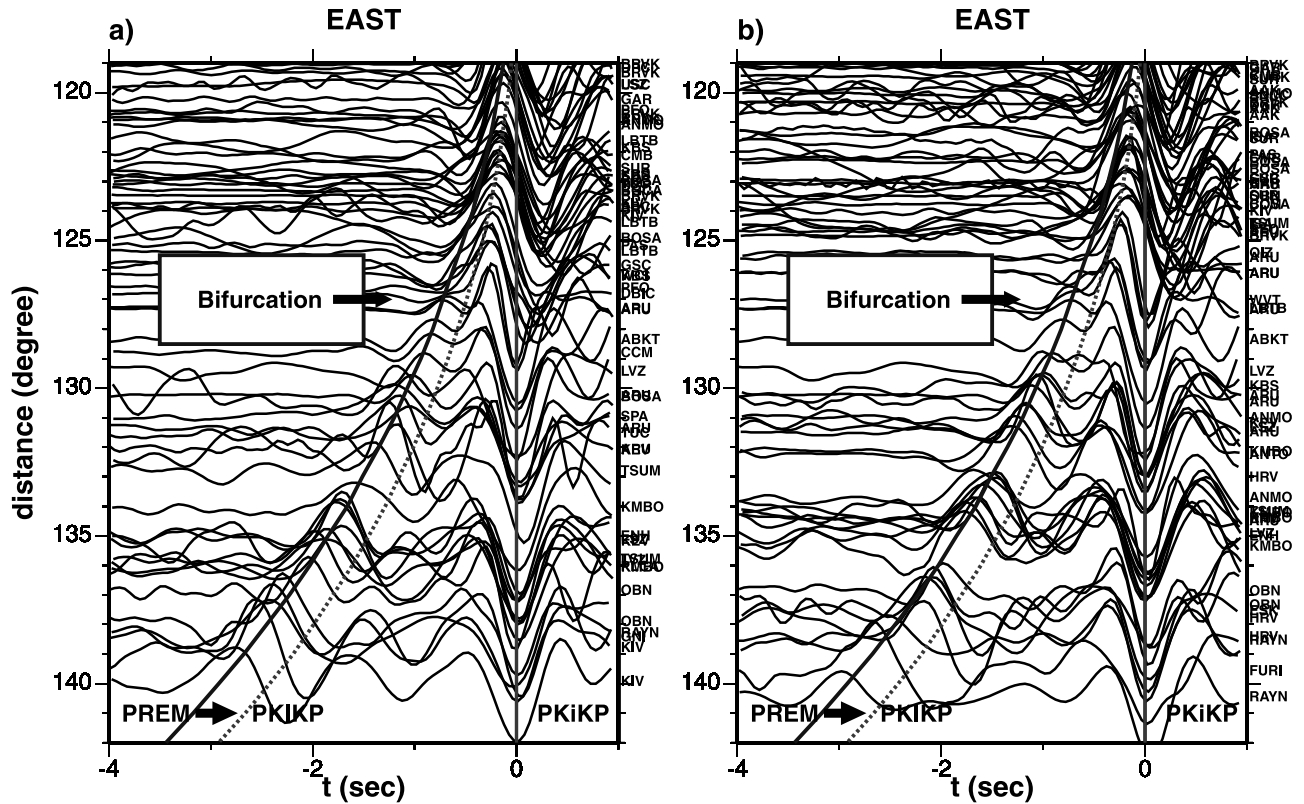


Figure 6. (a,b) Observed *PKIKP* and *PKiKP* phases sampling the eastern hemisphere; (c,d) the observations synthetics calculated for three models; and (e,f) a close look at the fitting of synthetics of different models to the data in the light blue boxes in Figures 6c and 6d (Figure 6e for the box in Figure 6c; Figure 6f for the box in Figure 6d). The seismic data are collected from the Global Seismic Network (see Figure 4 for great circle paths and the eastern hemisphere of the inner core sampled). All seismograms are processed and aligned as those in Figure 3c. Distance corrections are made so that all seismic data are aligned at the distances equivalent to a common source depth of 600 km. The dashed lines in Figures 6a and 6b are theoretical predicted arrivals based on PREM and the heavy lines mark approximately the arrivals observed in the *PKIKP* and *PKiKP* phases (their maximal amplitudes). Note that the data (heavy black traces) collected in the global seismic network show same characteristics as those recorded in the regional seismic networks (Figure 3c). Synthetics are calculated with model E1 (light red traces, Figures 6c–6f) and models with the W1 velocity gradient at the top of the inner core with *P* velocity jumps of 0.765 km/s (dashed blue traces, Figures 6c and 6e, model E11) and 0.732 km/s (dashed blue traces, Figures 6d and 6f, model E12), respectively. A source depth of 600 km is used in the synthetic calculations (Figures 6c–6f).

velocity structures assumed in the bottom of the outer core. For example, when we adopt a smaller radial velocity gradient (0.00023 (km/s)/km) in the bottom 20 km of the outer core, models W2 and E2 (Figures 8a and 8b) produce synthetic seismograms (dashed traces, Figure 3b for W2 and Figure 3d for E2) indistinguishable from those predicted by models W1 (heavy traces, Figure 3b) and E1 (heavy traces, Figure 3d). The velocity difference between E2 and W2 is the same as that between E1 and W1, although the velocity values at the top of the inner core change from 11.118 km/s (E1) to 11.085 km/s (E2) in the eastern hemisphere and from 10.986 km/s (W1) to 10.953 km/s (W2) in the western hemisphere (Figure 8a). Models E2 and W2, however, predict different absolute travel times from models E1 and W1 (Figure 9). The absolute velocity structures in the top of the inner core are theoretically resolvable from the *PKIKP* absolute travel times. We choose not to proceed further as absolute times would also be affected by many factors, such

as, mislocation of earthquake and seismic structures elsewhere. We instead emphasize the result of the relative difference of seismic velocity and *Q* structures between the two hemispheres.

[13] The different radial velocity gradients between the two hemispheres are tightly constrained by the observed waveform features. In Figure 6, we present “global” seismic observations (Figures 6a and 6b) sampling the eastern hemisphere of the inner core and compare them with synthetic seismograms (Figures 6c–6f) for model E1 and models with W1 radial velocity gradient in the top of the inner core. Because of the density of the data, we divide the data into two panels (Figures 6a and 6b or heavy black traces in Figures 6c and 6d), just for the displaying purpose. Model W1 is constrained by the observations sampling the western hemisphere (Figures 3a, 3b, and 5). Model E1 is also derived from the regional observations sampling the eastern hemisphere (Figures 3c and 3d). Model E11, with a *P* velocity

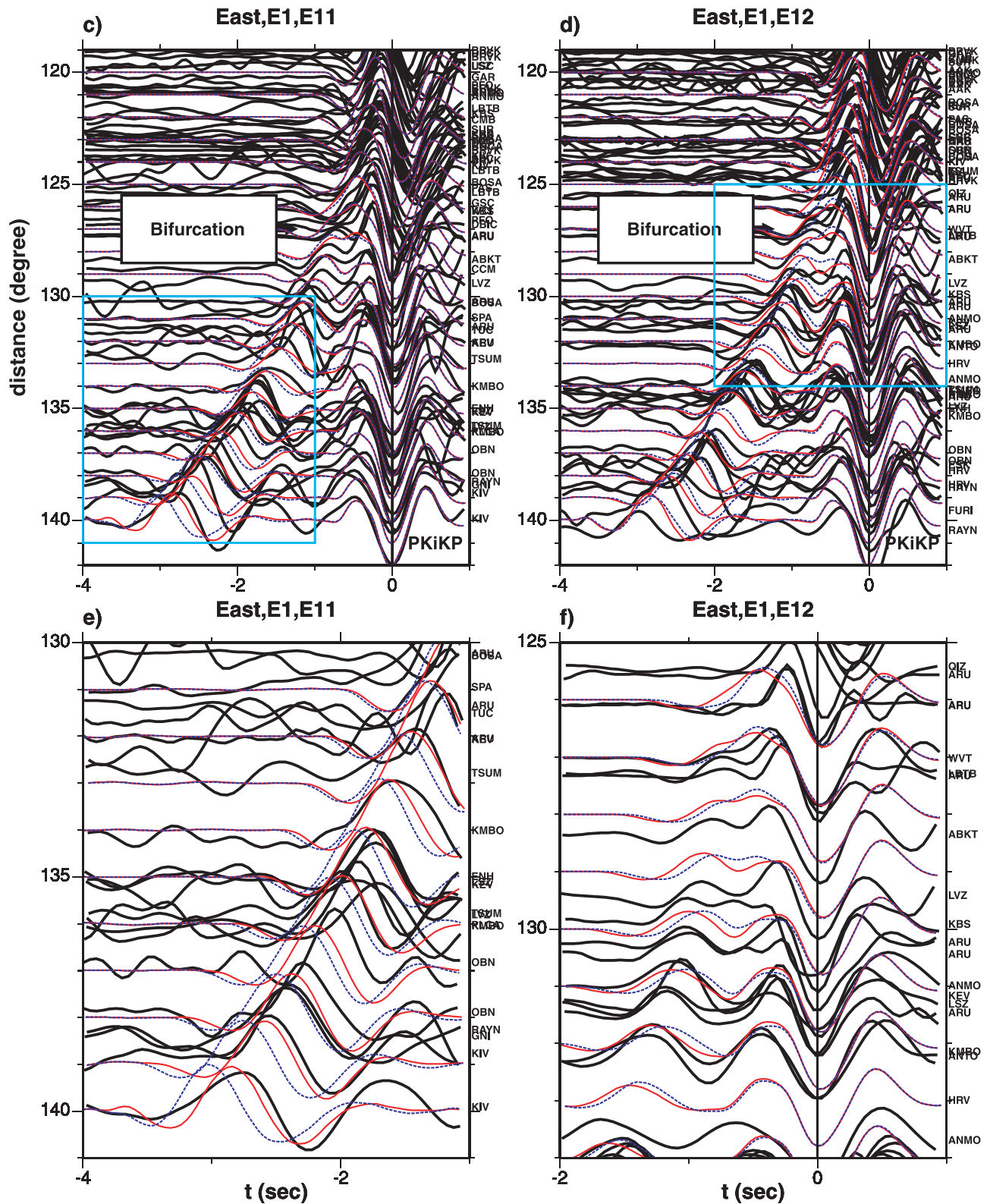


Figure 6. (continued)

jump of 0.765 km/s across the inner core boundary and W1 velocity gradient in the top of the inner core, explains the waveform features at the bifurcation distance range (125°–132°), but it predicts *PKiKP* phases earlier than those observed at large distances (dashed blue traces, Figure 6e).

Model E12, with a *P* velocity jump of 0.732 km/s across the inner core boundary and W1 velocity gradient in the top of the inner core, on the other hand, predicts correct timing for the observed *PKiKP* phases sampling the eastern hemisphere at large distances, but it fails to explain the waveform

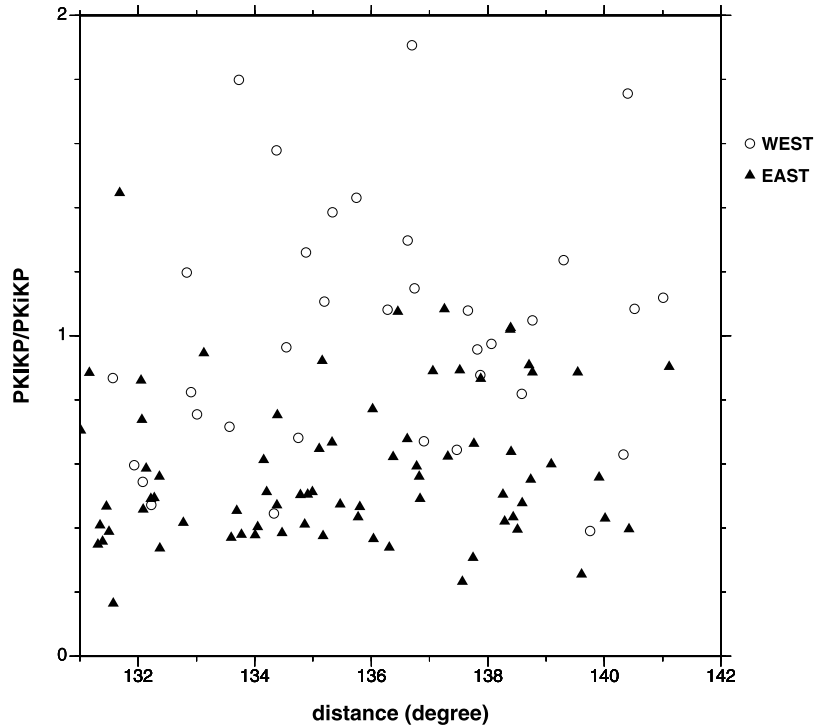


Figure 7. Observed $PKiKP/PKIKP$ amplitude ratios as a function of epicenter distance for seismic waves sampling the western (open circles) and the eastern (solid triangles) hemispheres of the inner core. Note that the $PKiKP/PKIKP$ amplitude ratios are systematically larger for seismic wave turning beneath the western hemisphere of the inner core.

features observed at the bifurcation distance range (125° – 132°) (dashed blue traces, Figure 6f).

[14] The attenuation structures are obtained by fitting the average observed relative $PKiKP/PKIKP$ amplitudes. In practice, to account for the effects of attenuation, we convolve $PKiKP$ synthetics with an attenuation operator t^* , which is the time integral of Q^{-1} along the ray path in the inner core. The hemispherical difference of attenuation structures is also resolved. For example, an average Q

value of 250, which is obtained by fitting the average $PKiKP/PKIKP$ amplitude ratios for the phases sampling the eastern hemisphere, would underpredict $PKiKP$ relative amplitudes for those sampling the western hemisphere (dashed traces, Figure 5b). The above Q values are obtained based on the assumption that the inner core boundary is a first-order discontinuity. The inferred values of attenuation may be affected by the transition thickness and the roughness of the inner core boundary. Short-period

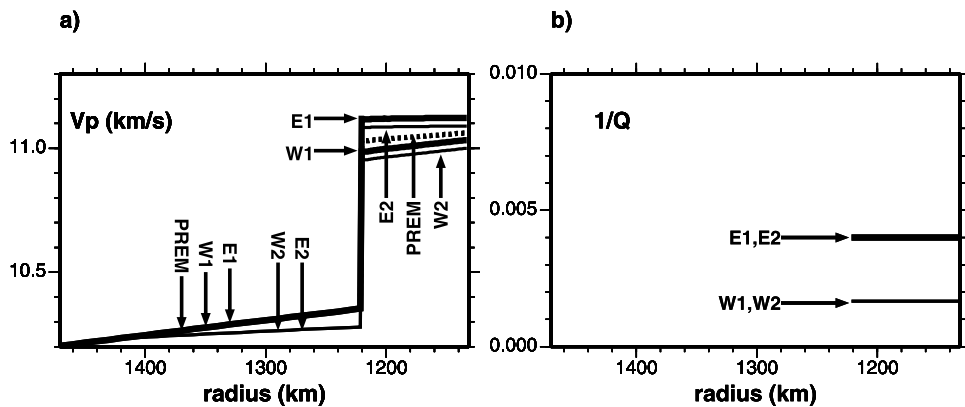


Figure 8. (a) One-dimensional seismic velocity and (b) Q models for the two hemispheres, with the synthetics shown in Figures 3b and 3d. E1, E2 are models for the eastern hemisphere of the top of the inner core, whereas W1, W2 are for the western hemisphere. E1, W1 have the same values as PREM (dashed line) in the outer core, whereas E2, W2 have a different velocity gradient in the bottom of the outer core. In the top of the inner core, the velocity difference between E2 and W2 is the same as that between E1 and W1.

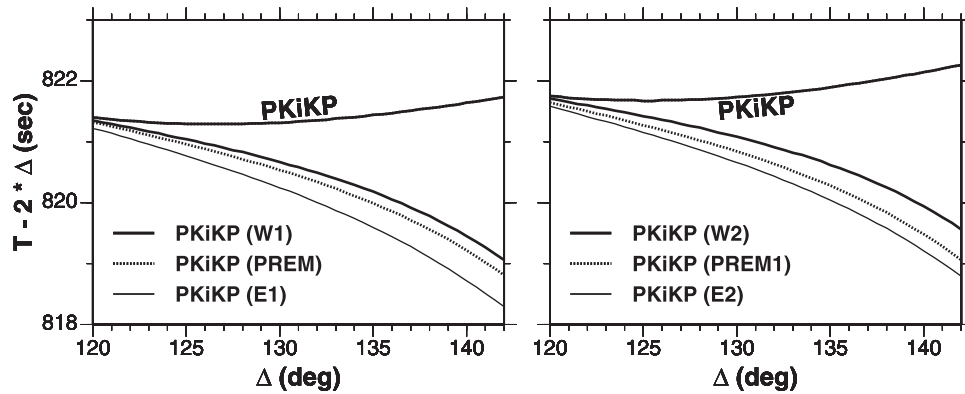


Figure 9. Travel time curves for *PKIKP* and *PKiKP* phases for six different models shown in Figure 8a. Note that although models W2 and E2 produce different absolute arrival times from models W1 and E1, the predicted differential *PKiKP*-*PKIKP* travel times between models W2 and E2 are the same as those between W1 and E1. PREM1 is a modified model from PREM with the velocity values of model E2 in the outer core.

seismic data collected at the distance range of 110° – 120° constrain the transition thickness of the inner core boundary to be less than 15 km, as such a transition thickness would produce complex waveforms which are not observed in the short-period seismic data sampling the both hemispheres. The predicted relative short-period *PKIKP*/*PKiKP* amplitudes are affected little within these allowable transitional thicknesses of the inner core boundary. As a result, our inferred Q values are affected little by using a first-order discontinuity to represent the inner core boundary. The roughness of the inner core boundary may also have effects on the *PKP* amplitudes. Unfortunately, we are hindered from addressing this issue because of our lack of knowledge of the roughness of the inner core boundary and seismic tools to deal with three-dimensional wave propagation in such high-frequencies.

[15] As an alternative to intrinsic attenuation, seismic scattering is also suggested as an explanation to the observed small amplitudes of *PKIKP* phase [Cormier *et al.*, 1998]. We consider this alternative by testing various random scattering models with different RMS variations of isotropic velocity. The seismic scattering indeed has similar effects as intrinsic attenuation: it reduces the amplitude and broadens the wave-shape of *PKIKP* phases (Figure 10). Not surprisingly, these effects are sensitive to the magnitude of seismic scatterers. In order to match the observed amplitudes of the *PKIKP* phases sampling the eastern hemisphere, the magnitude of RMS velocity variation is required to be between 5% and 9% in our two-dimensional modelings. On the other hand, the observations sampling the western hemisphere of the inner core require no scattering or scattering with little RMS variation of velocity ($<3\%$). We note that, however, the current scattering model produces synthetics (Figure 10d) which are broader than the data sampling the eastern hemisphere. Our goal here is not to search for a unique scattering model in the two-dimensional modeling. Rather, we place bounds on the magnitude of velocity variation required to explain the observed relative *PKP* amplitudes.

3. Discussion

[16] These seismic characteristics are important to our understanding of the nature of seismic anomalies in the top

of the inner core. (1) There exists a difference of seismic velocity and attenuation, with the magnitude of *P* velocity variation of 1.3%–0.8%, between the eastern and the western hemispheres and (2) the region of high velocities (the eastern hemisphere) has high attenuation or strong scattering.

3.1. Possible Interpretations

[17] A large-scale variation of temperature in the top of the inner core could unlikely explain the observed seismic structures for two reasons: (1) temperature variation is expected to be small (0.1–10 K) in the top of the inner core [Jeanloz and Wenk, 1988], the seismic anomaly associated with this magnitude of temperature variation is unlikely detectable from seismology and (2) temperature effect would predict high velocities correlating with low attenuation, opposite to our observations.

[18] Creager [1999] suggests that the variation of seismic velocity in the inner core is a result of different alignments of the anisotropic hcp-iron crystals rather than variations of temperature or composition. It is theoretically plausible that different alignments of the hcp-iron crystals could generate a velocity variation of 1.3%–0.8% between the two hemispheres, based on the available data about the seismic properties of the hcp-iron crystals [Stixrude and Cohen, 1995; Mao *et al.*, 1998, 1999]. For this mechanism to work, it would also require that the hcp-iron crystals are anisotropic in attenuation, with the direction of high attenuation corresponding to the direction of high velocity.

[19] Another possible explanation for the observed variations of seismic velocity and attenuation is existence of different geometric inclusions, and perhaps different fraction, of melt between the two hemispheres in the top of the inner core. The velocity and attenuation in a partially molten medium depend strongly on the fraction, geometry, and viscosity of the melt [Singh *et al.*, 2000]. It is plausible that different geometric inclusions of the melt between the “two hemispheres” generate a variation of *P* velocity of 1.3%–0.8%, a difference of attenuation and a correlation between high velocity with high attenuation [Singh *et al.*, 2000].

3.2. Possible Mechanisms

[20] We suggest that a large-scale (degree 1) heat flow anomaly at the bottom of the outer core might affect the

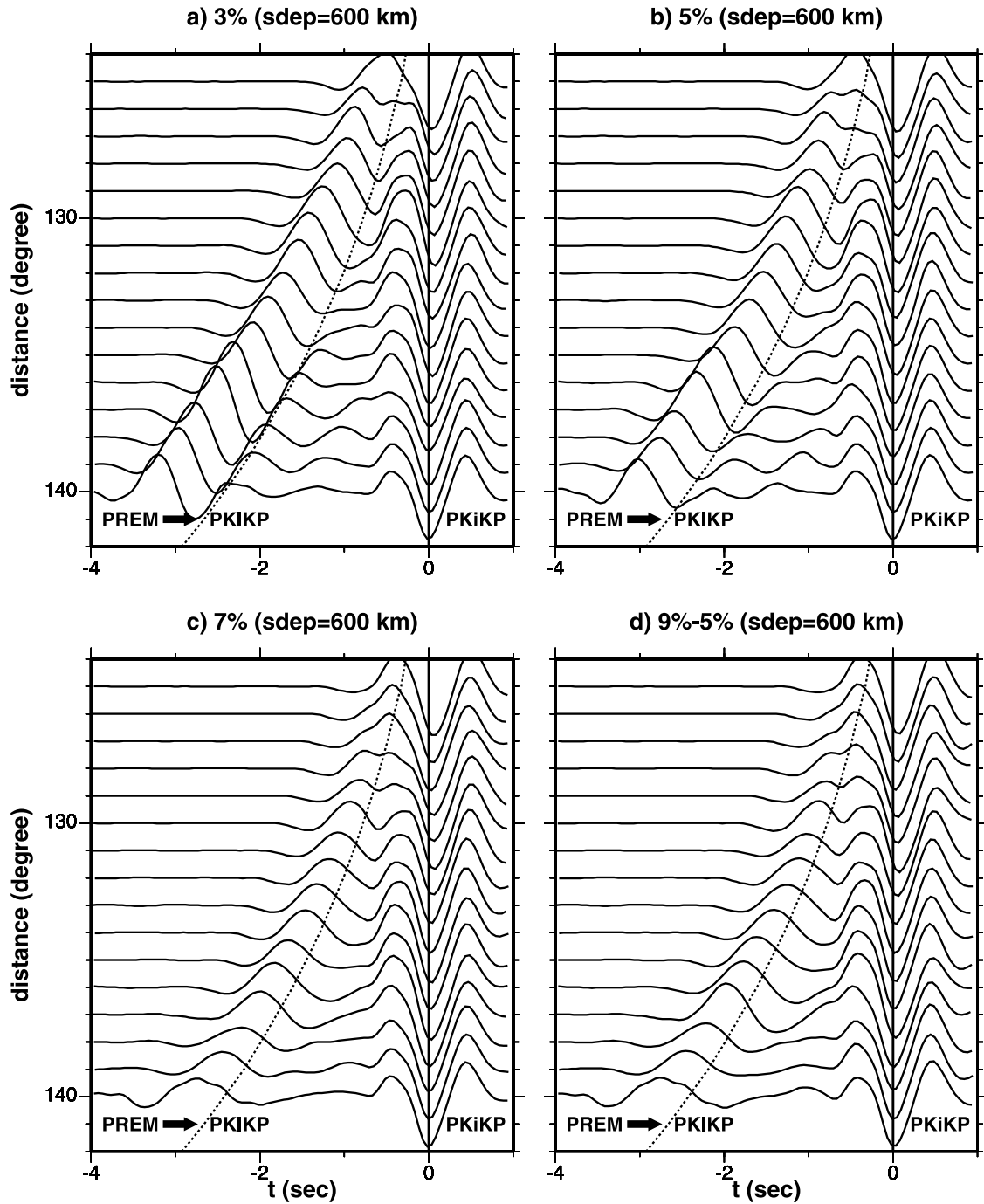


Figure 10. Synthetic seismograms for models with random scattering media with various RMS variations of P velocity and a correlation length scale of 1 km. (a–c) Synthetics for media of uniform random scattering with RMS variations of 3%, 5%, and 7%, respectively; (d) synthetics for a model with random scatterers with RMS variations varying from 9% in the inner core boundary to 5% in 100 km below the inner core boundary. Synthetics are calculated by hybrid method [Wen and Helmberger, 1998], with finite difference technique applied in the top of the inner core.

solidification of the inner core and thus produce the degree 1 pattern of seismic velocity in the top of the inner core [Niu and Wen, 2001]. In order for this mechanism to work, the large-scale heat flow should be able to sustain for a long period of time, because the solidification of the top 80 km of the inner core would probably take 80 Ma [Yoshida *et al.*, 1996]. One possibility is that this large-scale heat flow at the

bottom of the outer core is induced by a large-scale, relatively stable, heat flow at the core mantle boundary, similar to those observed in the laboratory experiments [Sumita and Olson, 1999].

[21] We further suggest that the degree 1 pattern of seismic structure may also be caused by thermal convection driven by internal heating in the top of the inner core. It has been

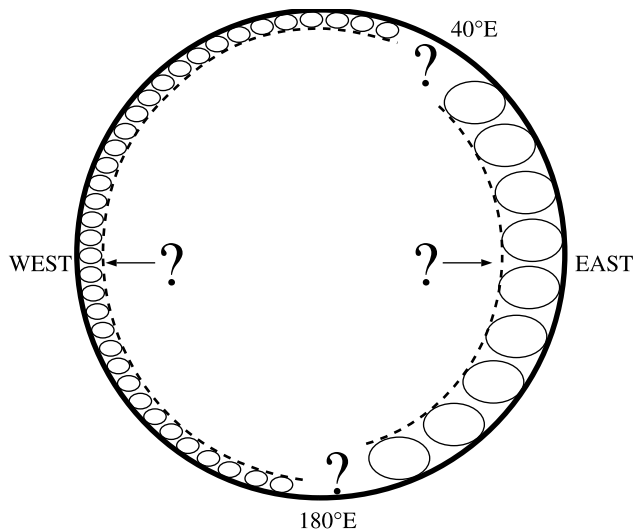


Figure 11. A cartoon indicating a possible scenario in the top of the Earth's inner core. A difference of vertical scale, viscosity, and heat resource in the western and eastern hemispheres results in different vigorousness of convection in the top of the two hemispheres. The different vigorousness of convection produces different geometric inclusions of melt and/or different alignments of iron crystals between the two hemispheres.

argued [e.g., *Yoshida et al.*, 1996], because of the highly incompatible nature of the radiogenic elements, that the very slow rates of crystallization of iron from the outer core would likely exclude the major radiogenic elements, such as U, Th, K, from the solid inner core. The lack of heat resource and the large thermal conductivity of iron crystals would likely prohibit convection in the inner core [e.g., *Yoshida et al.*, 1996]. However, if the top of the inner core is partially molten, radiogenic elements could coexist in the top of the inner core and convection is possible. It is, however, unclear how convection could generate a degree 1 pattern of flow, especially if the convection is confined in the top of the inner core and the vertical scales of the convection system are limited. Perhaps, a more reasonable explanation lies that a difference of vertical scale, viscosity and heat resource in the western and eastern hemispheres results in different vigorousness of convection in the top of the “two hemispheres” (Figure 11). The different vigorousness of convection produces different geometric inclusions of melt and/or different alignments of iron crystals between the two hemispheres. The existence of different viscosity and heat resource in the top of the two hemispheres is difficult to prove, but it is not an unreasonable assumption. The varying thickness of the top isotropic seismic layer between the eastern and western hemispheres is supported by various seismic studies [*Song and Helmberger*, 1998; *Tanaka and Hamaguchi*, 1997; *Creager*, 1999; *Garcia and Souriau*, 2000].

3.3. Implications to the Cause of Anisotropy in the Inner Core

[22] The hypothesis of convection in the top of the inner core does not exclude solidification texturing [*Bergman*, 1997] as a mechanism for the observed anisotropy in the deeper part of the inner core. It is possible that the real

solidification texturing takes place at the bottom of the isotropic seismic (convecting) layer, or convection disrupts the solidification texturing in the top of the inner core. If, however, vigorous convection in top of the inner core is required to generate the large-scale seismic heterogeneities we observed, it would probably exclude the anisotropy mechanisms appealing to the boundary forces at the inner core boundary, such as magnetic fields [*Karato*, 1999] and preferential growth of the inner core [*Yoshida et al.*, 1996]. Such boundary forces would likely be accommodated in the top convecting layer. Convection as a mechanism for the deep observed anisotropy [*Jeanloz and Wenk*, 1988; *Weber and Machetel*, 1992] still hinges on how much heat resource could reside in the deeper part of the inner core and how convection generates anisotropy with an axial symmetry.

4. Conclusion

[23] We collect a global data set of *PKIKP* and *PKiKP* phases recorded by the Global Seismic Network and many regional seismic arrays to study seismic structure in the top of the Earth's inner core. The *PKIKP* and *PKiKP* observations show different characteristics between those sampling the eastern hemisphere (40°E–180°E) of the inner core and those sampling the western hemisphere (180°W–40°E). *PKIKP* phases (1) arrive about 0.4 s earlier than the theoretical arrivals based on PREM for those sampling the eastern hemisphere of the inner core, and about 0.3 s later for those sampling the western hemisphere (131°–141°); (2) bifurcate at smaller epicentral distances for those sampling the eastern hemisphere, compared to those sampling the western hemisphere; and (3) have smaller amplitudes for those sampling the eastern hemisphere.

[24] Waveform modeling of these observations suggests two different types of models for the two hemispheres in the top of the inner core. The model in the eastern hemisphere has a *P* velocity increase of 0.765 km/s across the inner core boundary, a small radial velocity gradient of 0.000055 (km/s)/km, and an average *Q* value of 250, whereas the model in the western hemisphere has a *P* velocity increase of 0.633 km/s across the inner core boundary, a radial velocity gradient of 0.000533 (km/s)/km and an average *Q* value of 600. The difference of the inferred seismic velocities between the two hemispheres is independent of seismic structures assumed in the bottom of the outer core.

[25] The difference of seismic structures of the two hemispheres may be explained by different geometric inclusions of melt and/or different alignments of iron crystals with anisotropic properties in both seismic velocity and attenuation. We speculate that this large-scale pattern of seismic heterogeneities may be generated during solidification influenced by a large-scale heat flow anomaly at the bottom of the outer core, and/or different vigorousness of convection in top of the inner core between the two hemispheres.

[26] **Acknowledgments.** We are grateful to the IRIS, J-array Data Center, W. Shannon and L. Saumure of the Canadian National Seismic Network for supplying the data. Discussions with D. Weidner and W. Holt were helpful in preparing the manuscript. Annie Souriau, George Helffrich, an anonymous reviewer, and an Associate Editor provide constructive reviews, which improve the manuscript significantly. L.W. is supported by an NSF grant EAR 0001232. F.N. is supported by a fellowship of the Carnegie Institution of Washington.

References

- Anderson, O. L., Properties of iron at the Earth's core conditions, *Geophys. J. R. Astron. Soc.*, *84*, 561–579, 1986.
- Bergman, M. I., Measurements of electric anisotropy due to solidification texturing and the implications for the Earth's inner core, *Nature*, *389*, 60–63, 1997.
- Bhattacharyya, J., P. Shearer, and G. Masters, Inner core attenuation for short-period PKP(BC) versus PKP(DF) waveforms, *Geophys. J. Int.*, *114*, 1–11, 1993.
- Breger, L., H. Tkalcic, and B. Romanowicz, The effects of D'' on PKP (AB-DF) travel time residuals and implications for inner core structure, *Earth Planet. Sci. Lett.*, *175*, 133–143, 2000.
- Brown, J. M., and R. G. McQueen, Phase-transitions, Gruneisen-parameter, and elasticity for shocked iron between 77-GPa and 400-GPa, *Geophys. J. R. Astron. Soc.*, *91*, 7485–7494, 1986.
- Cormier, V. F., and G. L. Choy, A search for lateral heterogeneity in the inner core from differential travel times near PKP-D and PKP-C, *Geophys. Res. Lett.*, *13*, 1553–1556, 1986.
- Cormier, V. F., L. Xu, and G. L. Choy, Seismic attenuation of the inner core: Viscoelastic or stratigraphic?, *Geophys. Res. Lett.*, *25*, 4019–4022, 1998.
- Creager, K. C., Anisotropy of the inner core from differential travel times of the phases PKP and PKIKP, *Nature*, *356*, 309–314, 1992.
- Creager, K. C., Inner core rotation rate from small-scale heterogeneity and time-varying travel times, *Science*, *278*, 1284–1288, 1997.
- Creager, K. C., Large-scale variations in inner core anisotropy, *J. Geophys. Res.*, *104*, 23,127–23,139, 1999.
- Doornbos, D. J., The anelasticity of the inner core, *Geophys. J. R. Astron. Soc.*, *38*, 397–415, 1974.
- Dziewonski, A., and D. L. Anderson, Preliminary reference Earth model, *Phys. Earth Planet. Inter.*, *25*, 297–356, 1981.
- Fearn, D. R., D. E. Loper, and P. H. Roberts, Structure of the Earth's inner core, *Nature*, *292*, 232–233, 1981.
- Garcia, R., and A. Souriau, Inner core anisotropy and heterogeneity level, *Geophys. Res. Lett.*, *27*, 3121–3124, 2000.
- Helmburger, D. V., Theory and application of synthetic seismograms, in *Earthquakes: Observation, Theory and Interpretation*, edited by H. Kanamori, pp. 173–222, Soc. Ital. di Fis., Bologna, Italy, 1983.
- Jeanloz, R., and H. R. Wenk, Convection and anisotropy of the inner core, *Geophys. Res. Lett.*, *15*, 72–75, 1988.
- Kaneshima, S., Mapping heterogeneity of the uppermost inner core using two pairs of core phases, *Geophys. Res. Lett.*, *23*, 3075–3078, 1996.
- Karato, S.-I., Inner core anisotropy due to the magnetic field-induced preferred orientation of iron, *Science*, *262*, 1708–1711, 1993.
- Karato, S.-I., Seismic anisotropy of the Earth's inner core resulting from flow induced by Maxwell stresses, *Nature*, *402*, 871–873, 1999.
- Mao, H.-K., J. Shu, G. Shen, R. J. Hemley, B. Li, and A. K. Singh, Elasticity and rheology of iron above 220 GPa and the nature of the Earth's inner core, *Nature*, *396*, 741–743, 1998.
- Mao, H.-K., J. Shu, G. Shen, R. J. Hemley, B. Li, and A. K. Singh, Correction: Elasticity and rheology of iron above 220 GPa and the nature of the Earth's inner core, *Nature*, *399*, 280, 1999.
- McSweeney, T., K. C. Creager, and R. T. Merrill, Depth extent of inner-core seismic anisotropy and implications for geomagnetism, *Phys. Earth Planet. Inter.*, *101*, 131–156, 1997.
- Morelli, A., A. M. Dziewonski, and J. H. Woodhouse, Anisotropy of the inner core inferred from PKIKP travel times, *Geophys. Res. Lett.*, *13*, 1545–1548, 1986.
- Niu, F., and L. Wen, Hemispherical variations in seismic velocity at the top of the Earth's inner-core, *Nature*, *410*, 1081–1084, 2001.
- Poupinet, G., R. Pilet, and A. Souriau, Possible heterogeneity of the Earth's core deduced from PKIKP travel times, *Nature*, *305*, 204–206, 1983.
- Shearer, P. M., Axi-symmetric Earth's models for inner core anisotropy, *Nature*, *333*, 228–232, 1988.
- Shearer, P. M., Constraints on inner core anisotropy from PKP(DF) travel times, *J. Geophys. Res.*, *99*, 19,647–19,659, 1994.
- Singh, S. C., M. A. Taylor, and J. P. Montagner, On the presence of liquid in Earth's inner core, *Science*, *287*, 2471–2474, 2000.
- Song, X., and D. V. Helmburger, Anisotropy of the Earth's inner core, *Geophys. Res. Lett.*, *20*, 285–288, 1993.
- Song, X. D., and D. V. Helmburger, Depth dependency of anisotropy of Earth's inner core, *J. Geophys. Res.*, *100*, 9805–9816, 1995.
- Song, X., and D. V. Helmburger, Seismic evidence for an inner core transition zone, *Science*, *282*, 924–927, 1998.
- Souriau, A., and B. Romanowicz, Anisotropy in inner core attenuation: A new type of data to constrain the nature of the solid core, *Geophys. Res. Lett.*, *23*, 1–4, 1996.
- Souriau, A., and P. Roudil, Attenuation in the uppermost inner core from broadband Geoscope PKP data, *Geophys. J. Int.*, *123*, 572–587, 1995.
- Stixrude, L., and R. E. Cohen, High-pressure elasticity of iron and anisotropy of Earth's inner core, *Science*, *267*, 1972–1975, 1995.
- Su, W.-J., and A. M. Dziewonski, Inner core anisotropy in three dimensions, *J. Geophys. Res.*, *100*, 9831–9852, 1995.
- Sumita, I., and P. Olson, A laboratory model for convection in Earth's core driven by a thermally heterogeneous mantle, *Science*, *286*, 1547–1549, 1999.
- Sumita, I., S. Yoshida, M. Kumazawa, and Y. Hamano, A model for sedimentary compaction of a viscous medium and its application to inner core growth, *Geophys. J. Int.*, *124*, 502–524, 1996.
- Tanaka, S., and H. Hamaguchi, Degree one heterogeneity and hemispherical variation of anisotropy in the inner core from PKP(BC) - PKP(DF) times, *J. Geophys. Res.*, *102*, 2925–2938, 1997.
- Tromp, J., Support for anisotropy of the Earth's inner core from free oscillations, *Nature*, *366*, 678–681, 1993.
- Weber, P., and P. Machetel, Convection within the inner core and thermal implications, *Geophys. Res. Lett.*, *19*, 2107–2110, 1992.
- Wen, L., and D. V. Helmburger, A 2-D P-SV hybrid method and its application to modeling localized structures near the core-mantle boundary, *J. Geophys. Res.*, *103*, 17,901–17,918, 1998.
- Woodhouse, J. H., D. Giardini, and X.-D. Li, Evidence for inner core anisotropy from free oscillations, *Geophys. Res. Lett.*, *13*, 1549–1552, 1986.
- Yoshida, S., I. Sumita, and M. Kumazawa, Growth model of the inner core coupled with the outer core dynamics and the resulting elastic anisotropy, *J. Geophys. Res.*, *101*, 28,085–28,103, 1996.

F. Niu, Department of Terrestrial Magnetism, Carnegie Institution of Washington, 5241 Broad Branch Road, Washington, DC 20015, USA. (niu@dtm.civ.edu)

L. Wen, Department of Geosciences, State University of New York at Stony Brook, Stony Brook, NY 11794, USA. (Lianxing.Wen@sunysb.edu)